A Matrix Converter-Based Topology For High Power Electric Vehicle Battery Charging and V2G Application

Harish. S. Krishnamoorthy Pawan Garg Prasad. N. Enjeti
Department of Electrical & Computer Engineering, Texas A&M University, College Station, Tx-77843, USA
Email: enjeti@ece.tamu.edu

Abstract— **In this paper, a new three-phase converter topology based on a 3x1 matrix converter (MC) is proposed for Plug-in Hybrid or Battery (PHEV/BEV) electric transit buses. In the proposed approach, the MC directly converts the low frequency (50/60 Hz, three-phase) input to a high frequency (6 kHz, one-phase) AC output without a dc-link. The output of the matrix converter (MC) is then processed by a PWM rectifier via a high frequency (HF) isolation transformer to interface with the EV battery system. The MC-PWM rectifier system is made to operate like a dual active bridge (DAB), facilitating bi-directional power flow suitable for charging and Vehicle-to-Grid (V2G) application. The digital control of the system ensures that the input currents are of high quality under both charging and discharging operations. Due to the absence of dc-link electrolytic capacitors, power density of the proposed rectifier is expected to be higher. Analysis, design example and extended simulation results are presented for a three-phase 208 V_{LL}, 50kW charger.**

Keywords – Electric bus battery charger, High frequency transformer, Power factor correction, 3x1 Matrix Converter, V2G.

I. INTRODUCTION

Automobile and transportation sectors are constantly being subjected to tougher pollution standards and are urged to improve the e-mobility infrastructure of modern day vehicles. This has initiated a growing interest in the industry to build more electric vehicles (EVs). The commercial EVs can be hybrid (HEV), plug-in hybrid (PHEV) or battery (BEV) based on what the electric power train is designed for. The applications range from golf cart to fleet buses and trucks [1]. It has opened up an entirely new world of opportunities and challenges in power electronics' research [2]. Electric vehicles can potentially provide valued services to the power grid [3, 4]. The prospect of distributed regeneration (or microgrid) using EVs has further enhanced the opportunities by evolving the 'Vehicle-to-Grid' (*V2G*) frameworks to integrate electric vehicles into the grid and analyzing economic impact on the consumers and power grid [5-8].

The charging in EVs can be on-board or off-board. The chargers can vary in their power levels (normal-overnight, semi-fast and fast), charging modes (1-phase AC, 3-phase AC, DC, etc) and charging mechanisms (conductive or inductive). On-board AC charging offers flexibility and simplicity in the infrastructure as complicated communication protocol is not necessary. The normal or semi-fast chargers for electric cars are typically less than 10kW, 1-phase; whereas they can be more than 20kW, 3-phase for electric buses used in fleet. It takes 4-6 hours for full battery charging in the normal (overnight) power level. Research shows that hybrid/battery electric buses provide higher fuel economy, lower emissions and extended range compared to conventional diesel buses. If the system and maintenance costs are reduced, electric buses can be very attractive for the next generation commercial fleet [9]. Moreover if the concept of *V2G* becomes more prevalent in the future, the fleet owner can choose to transfer energy back to the grid when a bus is idle and improve the revenue.

A typical 3-phase isolated AC-DC converter consists of a 3-phase diode rectifier and an isolated DC-DC converter with high frequency (HF) transformer (see Fig. 1) [10]. These power supplies draw significant lower order harmonic currents from the utility, resulting in poor input power factor with high total harmonic distortion (THD), going even up to 40% [10]. This increases the input filter size required for smoothening the DC. The presence of multiple power conversion stages contributes to lower efficiency. Moreover, the entire system will have to be re-designed if V2G power conversion also needs to be considered [11].

More sophisticated converter configurations have also been proposed in the literature [11, 12]. Some concepts propose the use of current source rectifiers followed by inverter stage. This accounts for good input power quality, but still requires large electrolytic capacitors. The diodes in series with switches in a current source rectifier contribute to higher losses. Some other concepts involving multiple single phase power factor correction (PFC) stages [13], active power filters, line commutated rectifiers, etc. have also been proposed [11]. But all these add to the component count in the path of current that increases the overall system size and lowers the efficiency. The control of these converters leads to larger system complexity.

In order to overcome the drawbacks of the existing 3-phase high power PHEV/BEV battery charging power supplies, a new matrix converter (MC) based architecture has been proposed in this paper that can also support V2G power transfer (see Fig. 2). With the availability of faster power semiconductor devices, MCs have become more efficient and simpler to design. The 3-phase utility power input is fed to a 3x1 MC through an LC filter. This converts the utility grid voltage to single-phase high frequency (HF) square wave, which is interfaced to a HF transformer, followed by a PWM rectifier. The rectifier's phase shift is controlled to regulate the

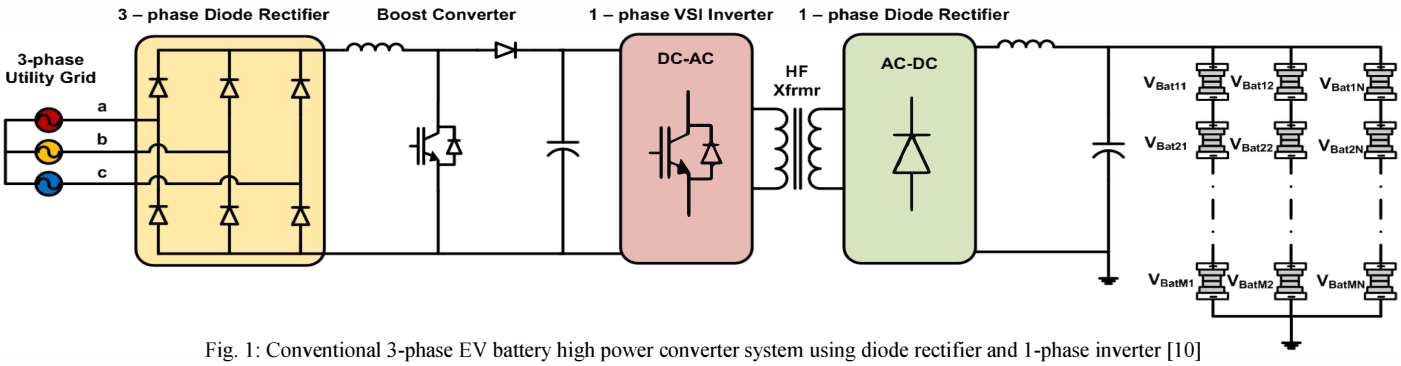

Fig. 1: Conventional 3-phase EV battery high power converter system using diode rectifier and 1-phase inverter [10]

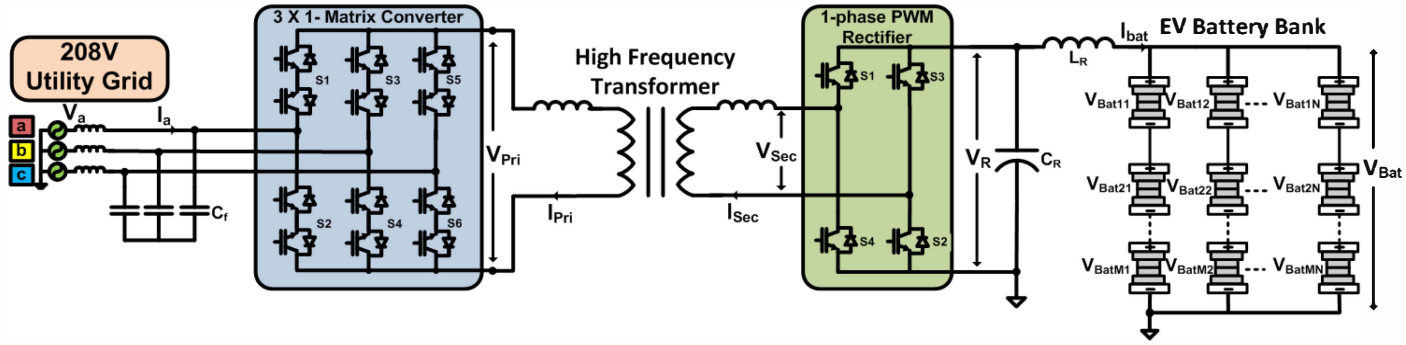

Fig. 2: Proposed 3-phase EV battery charging power converter system using 3x1 Matrix Converter based dual active bridge

battery DC current. The advantages of the proposed EV power converter topology are as follows:

- The proposed topology allows for bi-directional power flow between grid and EV battery bank, facilitating V2G infrastructure.
- The use of a high-frequency-link transformer provides galvanic isolation and also reduces the system size [11].
- MCs being direct AC-AC converters, there is no need for an electrolytic capacitor on the converter side, which increases the converter power density, reliability and reduces the size.
- The input power factor (PF) can be regulated to near unity.
- The PWM rectifier operated in high-frequency square wave phase-shift mode produces a high-quality DC output that makes the DC-link filter size small.
- As the charge is regulated in the current control mode, the battery current is high quality and the control loop is robust.

II. Proposed Electric Vehicle Battery Charging System with Matrix Converter

The design of the entire topology in Fig. 2 can be mainly divided into the following sections: (i) 3x1 Matrix Converter (MC) (ii) High Frequency (HF) Transformer, (iii) 1-phase PWM Rectifier (iv) Filter Design and (v) Control Scheme.

(i) 3 x 1 Matrix Converter

The MC converts the 3-phase utility grid AC to 1-phase HF AC. The converter is made up of six bidirectional switches as shown in Fig. 2. A 3x1 MC operation can be illustrated by separating it into a rectifier, a fictitious DC link and a 1-phase inverter as shown in Fig. 3. The rectifier can be operated as a diode rectifier or a current source based PWM rectifier (CSR). The latter is chosen as it gives better input power quality. The fictitious DC is assumed to be a large DC inductor. The inverter is operated in voltage source mode (VSI). The two converters are bridged by a fictitious DC link current, $\boldsymbol{I_{dc}}$.

The switching scheme for the MC is a product of a unipolar sinusoidal PWM (obtained by interfacing a sinusoidal wave of frequency $\boldsymbol{f_s}$ with the triangular carrier wave of frequency $\boldsymbol{f_c}$ as in a CSR) and a HF square wave ($\boldsymbol{f_{sq}}$) [14]. The entire switching scheme is explained by (1-6). A bipolar line-to-neutral wave S_A is created when the reference sine wave, S_{grid} with frequency f_{grid} overlays the triangular carrier wave S_c with frequency f_c. The signal and carrier signals are described by (1) and (2), respectively.

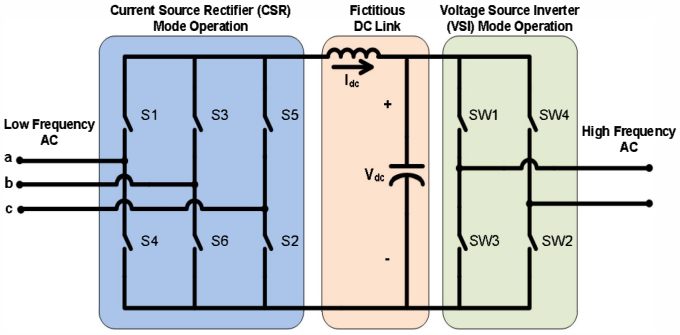

Fig. 3: 3x1 Matrix Converter illustration [10]

$$S_{grid} = m_a \cdot \sin\left(2\pi f_{grid} \cdot t\right) \quad (1)$$

$$S_c = \frac{8}{\pi^2} \cdot \sum_{n=1,3,5\ldots}^{\infty} \frac{(-1)^{\frac{(n-1)}{2}}}{n^2} \cdot \sin(n \cdot 2\pi f_c \cdot t) = sinc^2(f_c) \quad (2)$$

S_A is the PWM signal generated using (1) and (2) and is represented in (3). Here, $m_a = \hat{V}_{grid} / \hat{V}_c$ and $m_f = f_c / f_{grid}$.

$$S_A = \frac{m_a}{2} \cdot \begin{bmatrix} \sin(2\pi f_{grid} \cdot t) + 0.601 \sin(2\pi \cdot \{m_f\} \cdot f_{grid} \cdot t) \\ + 0.318 \sin(2\pi \cdot \{m_f \pm 2\} \cdot f_{grid} \cdot t) \\ + 0.018 \sin(2\pi \cdot \{m_f \pm 4\} \cdot f_{grid} \cdot t) \\ + 0.181 \sin(2\pi \cdot \{2m_f \pm 1\} \cdot f_{grid} \cdot t) \\ + 0.212 \sin(2\pi \cdot \{2m_f \pm 3\} \cdot f_{grid} \cdot t) \\ + 0.033 \sin(2\pi \cdot \{2m_f \pm 5\} \cdot f_{grid} \cdot t) \\ + higher\ order\ terms \end{bmatrix} \quad (3)$$

In (4), a unipolar line-to-line switching function S_{AB} is created by taking the difference between S_A and S_B (S_{AB} is similar to a CSR signal [15]), which are 120° out of phase. Unipolar switching is chosen because it allows the sum of phase currents to be zero at every instant. This is not the case with bipolar switching, where the sum of currents can be either $\pm\hat{\boldsymbol{I}}_{\boldsymbol{dc}}$. Here, m_a is assumed to be unity, to maximize converter gain. Moreover, the use of space vector modulation (SVPWM), 3rd harmonic injection or selective harmonic elimination method can further extend the gain up to around 15%. Fig. 4 (a) - (c) shows sample unipolar line-to-line switching functions of a PWM CSR and the fundamental.

$$S_{AB} = m_a \cdot \begin{bmatrix} 0.612 \sin(2\pi f_{grid} \cdot t) \\ + 0.195 \sin(2\pi \cdot \{m_f \pm 2\} \cdot f_{grid} \cdot t) \\ + 0.011 \sin(2\pi \cdot \{m_f \pm 4\} \cdot f_{grid} \cdot t) \\ + 0.111 \sin(2\pi \cdot \{2m_f \pm 1\} \cdot f_{grid} \cdot t) \\ + 0.020 \sin(2\pi \cdot \{2m_f \pm 5\} \cdot f_{grid} \cdot t) \\ + higher\ order\ terms \end{bmatrix} \quad (4)$$

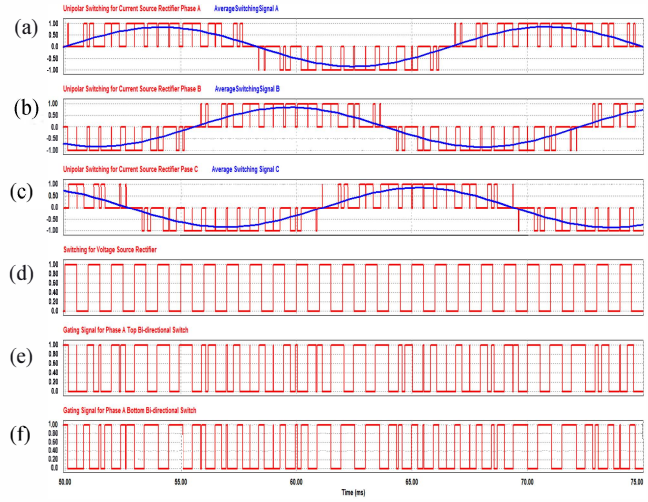

Fig. 4: Switching Scheme for Matrix Converter (a) – (c) Unipolar switching for Current Source Rectifier for phase A-C, (d) Switching for Voltage Source Inverter, (e) Gating signal for Phase A (top) bi-directional switch and (f) Gating signal for Phase A (bottom) bi-directional switch

The VSI switching function, used for the signal multiplication, is square wave S_{sq} with frequency f_{sq} is given by (5) and is shown in Fig. 4 (d). In this work the value of f_{sq} has been chosen as 6 kHz and value of f_c has been chosen to be 24 kHz. It is significant to note that this value is limited by the transformer core material for the particular power rating. The transformer is discussed in more detail in section (ii). Finally, the resulting switching function for MC, $S_{ac/ac}$ is given by multiplying the line-to-line switching function with the VSI switching function, as in (6). Gating signals to the top and bottom switches of MC leg for phase-A have been shown in Fig. 4 (e) and (f), respectively.

$$S_{sq} = \frac{4}{\pi} \cdot \hat{V}_{sq} \sum_{n=1,3,5\ldots}^{\infty} \frac{1}{n} \sin(n \cdot 2\pi f_{sq} \cdot t) \quad (5)$$

$$S_{ac/ac} = S_{AB} * S_{sq} \quad (6)$$

The resulting switching function is used to gate the MC switches. In this case, the multiplication of switching functions get translated as logical XOR or AND operations [10] between line-to-line gating signals and VSI square gating signals. The switching logic has been explained for each leg of the matrix converter in the Table 1-3. It may be noted that the MC switching works in such a way, that when all the line-to-line gating signals are zero, one of the legs of the MC is shorted to provide a free-wheeling path for the transformer current. This helps in reducing the undue voltage spikes due to high $\frac{di}{dt}$.

Table 1 : Gating signals for Leg A

	$S_{AB} = 1$	$S_{AB} = -1$	$S_{AB} = 0$
$S_{sq} = 1$	V_{gA+}=1 V_{gA-}=0	V_{gA+}=0 V_{gA-}=1	V_{gA+}=0 V_{gA-}=0
$S_{sq} = 0$	V_{gA+}=0 V_{gA-}=1	V_{gA+}=1 V_{gA-}=0	V_{gA+}=0 V_{gA-}=0

Table 2 : Gating signals for Leg B

	$S_{BC} = 1$	$S_{BC} = -1$	$S_{BC} = 0$
$S_{sq} = 1$	V_{gB+}=1 V_{gB-}=0	V_{gB+}=0 V_{gB-}=1	V_{gB+}=0 V_{gB-}=0
$S_{sq} = 0$	V_{gB+}=0 V_{gB-}=1	V_{gB+}=1 V_{gB-}=0	V_{gB+}=0 V_{gB-}=0

Table 3 : Gating signals for Leg C

	$S_{CA} = 1$	$S_{CA} = -1$	$S_{CA} = 0$
$S_{sq} = 1$	V_{gC+}=1 V_{gC-}=0	V_{gC+}=0 V_{gC-}=1	V_{gC+}=0 V_{gC-}=0
$S_{sq} = 0$	V_{gC+}=0 V_{gC-}=1	V_{gC+}=1 V_{gC-}=0	V_{gC+}=0 V_{gC-}=0

Overall, the MC converter switching will be able to de-couple the input current frequency components and the transformer voltage frequency components in such a way that the input current harmonics can be of much higher order whereas the transformer can be of the required HF. It should be noted that in the proposed system, 3 x 1 MC is operating under balanced voltage in open loop, with just a synchronizing reference signal. So, the implementation of switching scheme is straightforward.

(ii) High Frequency Transformer

High frequency (HF) transformer forms a very critical portion of the system. While a 60Hz transformer is bulky, a HF transformer can pose challenges in terms of hysteresis, eddy current and skin affect losses. So the selection of appropriate transformer core becomes very important to avoid these losses. Amorphous alloys, ferrite, powdered iron and Nano-crystalline offer high performance characteristics for transformer core at frequencies in the range of 3 kHz to 20 kHz [16]. Powdered iron core has been popularly accepted as a viable solution for EV application and can be employed for the design of the 6 kHz transformer used [2].

In order to calculate the turns-ratio of the transformer, the peak value of square wave at the primary has to be considered. Operating the MC in CSR-VSI mode, the peak amplitude of the square wave can be calculated by:

$$V_{pk} = \left(\frac{\sqrt{3}}{2} * \frac{3\cdot\sqrt{2}}{\pi}\right) \cdot V_{grid,LL} \quad (7)$$

At utility input of $208V_{grid,LL}$, the peak value can be calculated as 244V. As the battery voltage on the secondary side can fluctuate from $450V_{dc}$ to $250V_{dc}$ in a high power EV charger, the turns-ratio is taken as **8:15** for optimum control.

(iii) 1-Phase PWM Rectifier

The PWM rectifier used in the secondary side of the high isolation transformer is made to operate with square wave PWM at the same frequency as f_s (6 kHz). This is based on the principle that multiplication of a square wave with the same square wave will result in a DC voltage.

When the square signal is high, switches on the leading diagonal of the rectifier are turned on and when the square wave is zero, the other two switches are turned on. The square wave modulated PWM rectifier is operated in closed loop so as to regulate the battery DC current. The control system is discussed in detail in Section (v).

(iv) Filter Design

The input filter has to be designed to restrict the switching frequency (24 kHz) and higher order harmonics in input current to keep the Total Harmonic Distortion (THD) less than 5%. The filter has been designed using equivalent circuit models, shown in Fig. 5 and Fig. 6.

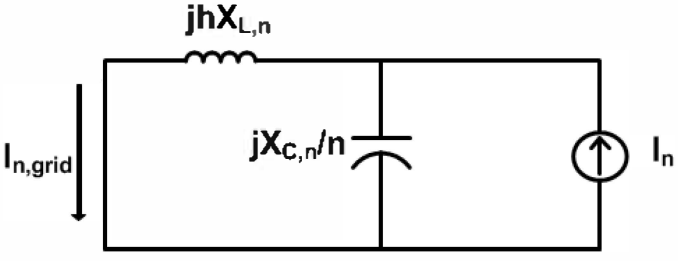

Fig. 5: Input Filter design illustration

The values for input filter inductor and capacitor obtained from calculations as per Fig. 5 are:

$$C_f = 150\mu F$$
$$L_f = 30\mu H$$

In addition to the input filter, the output filter also needs to be designed to restrict the second harmonic frequency (12 kHz) and higher order harmonics in battery current to less than 15% of DC current (see Fig. 6). Based on the calculations, the following values have been used:

$$C_R = 220\mu F$$
$$L_R = 80\mu H$$

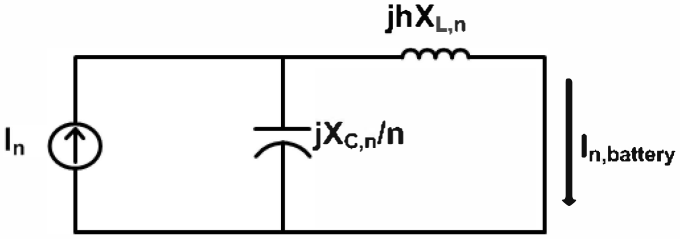

Fig. 6: Output filter design illustration

(v) Control Scheme

The matrix converter on the primary side of the transformer operates synchronously with utility voltage and the square wave modulated PWM rectifier on the secondary side operates in closed loop, regulating the battery current- I_{bat}. The controller regulating the power flow is located on the secondary side of the transformer. It senses the DC current to the EV battery bank and adjusts (using a PI controller) the phase-shift of the PWM rectifier modulation with respect to the transformer primary voltage, in order to regulate the current as required. The matrix converter and PWM rectifier form a dual active bridge [17]. The entire control scheme is shown in Fig. 7.

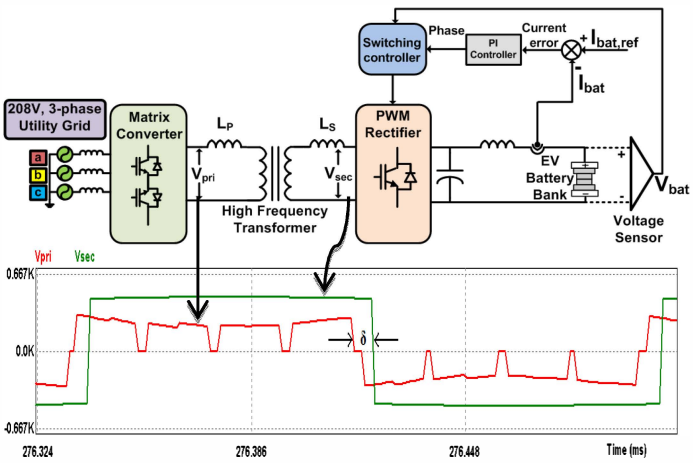

Fig. 7: Control scheme based on the Dual Active Bridge phase control (showing voltage at primary and phase shifted input of the rectifier)

As the secondary is a PWM rectifier instead of a diode rectifier used in conventional topologies, there can be a bi-directional power flow. Another advantage is that there is complete isolation between primary and secondary side control strategy, as no signal from the transformer primary is required on the secondary side to regulate the power flow.

III. Simulation Results

The proposed system has two modes of operation, (1) Charging & (2) V2G: Discharging. Simulations have been carried out for both these modes. In addition to these conditions, performance of the system has been simulated for (3) varying output voltage to emulate charging of a battery and (4) under the condition of sudden variation in set-point. The results are presented in this section.

1. Charging operation

Fig. 8 shows the result for EV battery bank charging operating mode. Fig. 8 (a) shows the battery current (I_{bat}) and voltage (V_{bat}). I_{bat} was regulated at 100A at a battery voltage of 450V. As evident, the DC battery current is of good quality (ripple < 15%). Fig. 8 (b) shows the utility phase-A voltage (V_a) and phase-A current drawn by the system (I_a). The input power factor is > 0.99. The currents in other phases also follow similar waveform. Fig. 8 (c) shows the transformer secondary current (I_{sec}). The Fig. 9 shows FFT of waveforms in Fig. 8. It can be seen that the transformer current is of high frequency (6kHz). Due to the leakage inductance in the transformer, the transformer current has some transients

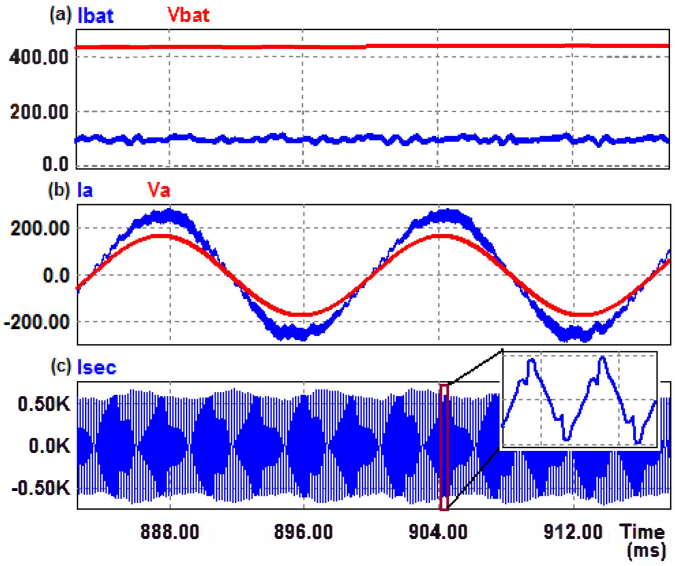

Fig. 8: Charging operation (a) DC current into the battery and battery voltage, (b) Grid phase-A current and voltage and (c) Transformer current on the secondary side

2. V2G: Discharging operation

As discussed before, the proposed system is capable of bi-directional power transfer. The system performance during power transfer from vehicle to grid (V2G), i.e. discharging operation, is shown in Fig. 10. The negative battery current in Fig. 10 (a) and the 180° phase shift between the grid phase-A voltage and current in Fig. 10 (b) make it evident that power is being transferred to the grid. It may be noted that the magnitude of DC current required during V2G operation is smaller than that during charging operation. It is generally done to avoid rapid dumping of energy onto the grid and to reduce the wear and tear in the battery system. But it can be seen from Fig. 10 that the proposed converter can handle large currents even during V2G operation.

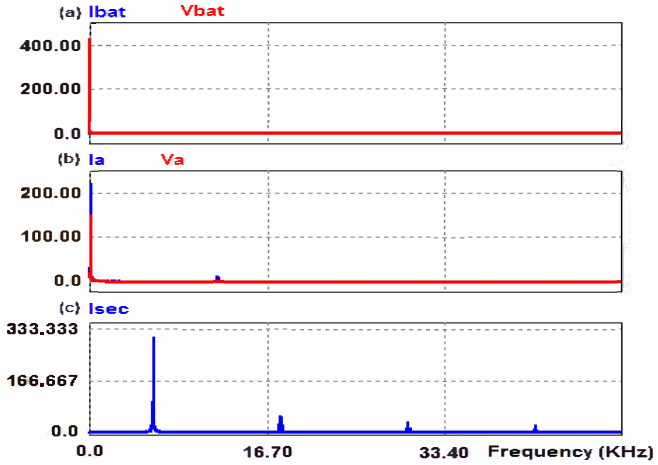

Fig. 9: Frequency spectrum (FFT) of waveforms in Fig. 8

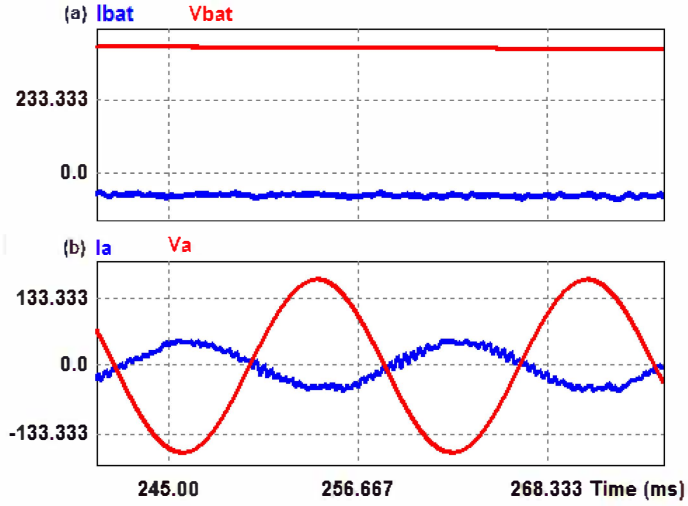

Fig. 10: Discharging operation (a) Battery current and voltage, and (b) Grid phase-A current and voltage

3. Variable output DC voltage

As the battery charges, the output voltage will increase. To check the performance in this case, the battery bank was simulated as a large capacitor ($C \approx 0.1\ F$). As observed from Fig. 11, the controller is able to regulate current in case of increasing output voltage (shown in Fig. 11 (a) from 375V to 450V). During charging at constant current, the battery voltage increases. In order to supply this increased power, the utility grid currents also have to increase. The charging currents are varied depending on the State of Charge (SOC) in the battery for storing the maximum possible energy in the cells.

4. Step response of controller

The step response of the controller is shown in Fig. 12. A step change of DC current set-point from 100A to 40A (with a time constant of 0.1 seconds) was provided to observe the stability of the control scheme (see Fig. 12 (a)). It can be seen that control scheme keeps the system stable even at such fast changes in battery current reference. Fig. 12 (b) shows that the utility grid current (I_a) magnitude reduces with battery current

and yet maintains near unity power factor. In practical applications, though any such rapid changes in current set-point are not expected, this experiment shows that the proposed control scheme is robust enough to handle sudden changes in set-point.

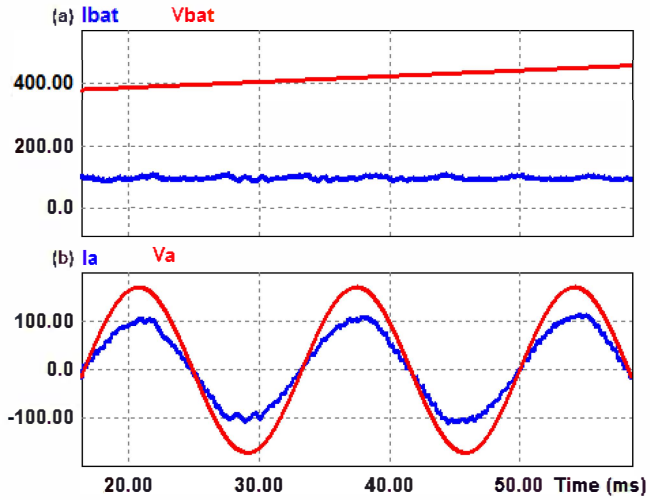

Fig. 11: DC Current regulation during battery charging (Battery emulated with a large capacitor=0.1F) (a) Battery DC current and voltage, and (b) utility grid phase-A current and voltage

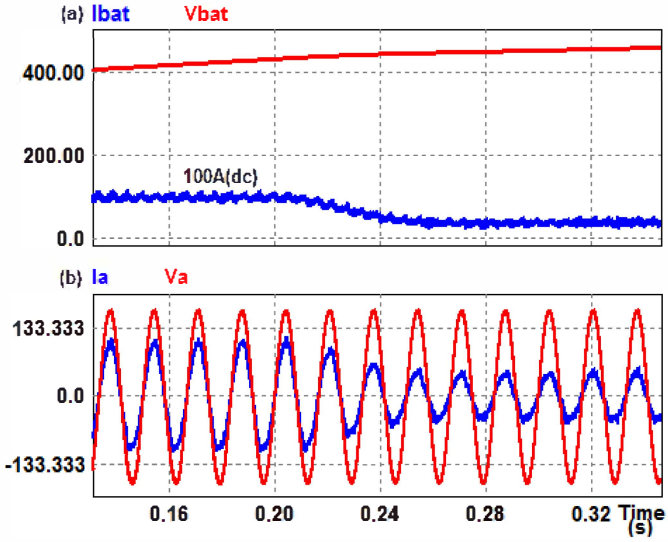

Fig. 12: Step response of control scheme (a) Battery current and voltage, and (b) Grid phase-A current and voltage

IV. Conclusion

A new high power rectifier topology was introduced in this paper for electric transit bus battery charging. The theoretical analysis, calculations and simulation results were discussed in detail, along with the advantages of the system. It is seen that the proposed converter has the potential to enhance the performance and efficiency of power conversion in high power electric bus battery charging and V2G power conversion. The topology reduces the overall system size and increases the power density, making it suitable for on-board battery charging. This is achievable due to the HF transformer and elimination of electrolytic capacitors from the primary side power conversion. Moreover, V2G operation can be performed with the same ease as charging operation in the MC based topology; which makes the converter even more attractive for commercial EV infrastructure.

VI. References

1. Association, N.E.C., *Draft Standard: Standard for Installing and Maintaining Electric Vehicle Supply Equipment (EVSE)*, 2011.
2. Aggeler, D., et al. *Ultra-fast DC-charge infrastructures for EV-mobility and future smart grids.* in *Innovative Smart Grid Technologies Conference Europe (ISGT Europe), 2010 IEEE PES.* 2010.
3. Kempton, W. and S.E. Letendre, *Electric vehicles as a new power source for electric utilities.* Transportation Research Part D: Transport and Environment, 1997. **2**(3): p. 157-175.
4. Tu, Y., et al. *Research on Vehicle-to-Grid Technology.* in *Computer Distributed Control and Intelligent Environmental Monitoring (CDCIEM), 2011 International Conference on.* 2011.
5. Guille, C. and G. Gross, *A conceptual framework for the vehicle-to-grid (V2G) implementation.* Energy Policy, 2009. **37**(11): p. 4379-4390.
6. Kempton, W. and J. Tomić, *Vehicle-to-grid power fundamentals: Calculating capacity and net revenue.* Journal of Power Sources, 2005. **144**(1): p. 268-279.
7. Kempton, W. and J. Tomić, *Vehicle-to-grid power implementation: From stabilizing the grid to supporting large-scale renewable energy.* Journal of Power Sources, 2005. **144**(1): p. 280-294.
8. Kramer, B., S. Chakraborty, and B. Kroposki. *A review of plug-in vehicles and vehicle-to-grid capability.* in *Industrial Electronics, 2008. IECON 2008. 34th Annual Conference of IEEE.* 2008.
9. Chandler, K., K. Walkowicz, and L. Eudy. *New York City Transit Diesel Hybrid-Electric Buses: Final Results.* 2002 [cited 2012; Available from: http://www.afdc.energy.gov/pdfs/nyct_diesel_hybrid_final.pdf.
10. S. Ratanapanachote, H.J.C., P. Enjeti, *A digitally controlled switched mode power supply based on Matrix Converter.* IEEE Power Electronics Transactions, January 2006. **21**(1): p. 124-130.
11. Soeiro, T., T. Friedli, and J.W. Kolar. *Three-phase high power factor mains interface concepts for Electric Vehicle battery charging systems.* in *Applied Power Electronics Conference and Exposition (APEC), 2012 Twenty-Seventh Annual IEEE.* 2012.
12. Kang, M., P.N. Enjeti, and I.J. Pitel, *Analysis and design of electronic transformers for electric power distribution system.* Power Electronics, IEEE Transactions on, 1999. **14**(6): p. 1133-1141.
13. Chapman, D., D. James, and C.J. Tuck. *A high density 48 V 200 A rectifier with power factor correction-an engineering overview.* in *Telecommunications Energy Conference, INTELEC '93. 15th International.* 1993.
14. Krishnamoorthy, H.S., et al. *A new multilevel converter for Megawatt scale solar photovoltaic utility integration.* in *Applied Power Electronics Conference and Exposition (APEC), 2012 Twenty-Seventh Annual IEEE.* 2012.
15. Mohan, N., T.M. Undeland, and W.P. Robbins, *Power electronics : converters, applications, and design.* 3rd ed. 2003, Hoboken, NJ: John Wiley & Sons. xvii, 802 p.
16. Leung, C.-k., *Design Considerations of High Voltage and High Frequency 3 Phase Transformer for Solid State Transformer Application*, in *Electrical Engineering*2010, North Carolina State University: Raleigh, North Carolina.
17. Kheraluwala, M.N., et al., *Performance characterization of a high-power dual active bridge.* Industry Applications, IEEE Transactions on, 1992. **28**(6): p. 1294-1301.